HIGH ENTROPY ALLOY AT HIGH TEMPERATURE AND PRESSURE

Abdullah Al Masum Jabir[1, *] and Farjana Jahan[2]
[1]Graduate Research Assistant,
Department of Industrial and Manufacturing Engineering,
University of Texas Rio Grande Valley, Edinburg, TX
Email: masum.jabir@gmail.com
[2]Graduate Assistant, Department of Statistics,
Western Michigan University, Kalamazoo, MI
Email: jfarjana475@gmail.com

ABSTRACT

In recent times, high-entropy alloys (HEAs) have gained significant recognition as metallic materials owing to their distinctive design approaches and exceptional mechanical characteristics. HEA consists of five principal elements or more. Due to having more elements, there are four core effects observed in HEA. These four core effects are the driving force for giving unique mechanical properties. So, developing those HEAs in order to applied in the extreme condition becomes a new attraction. Refractory HEAs (RHEAs) are regarded as a novel class of materials that exhibit exceptional mechanical properties at high temperature. These alloys hold significant promise for replacing nickel-based superalloys. We reviewed the history of the HEAs. Main four core effects. The microstructure and phase transition at high pressure. Refractory HEAs microstructure and mechanical properties at high temperature.

KEYWORDS: *High Entropy Alloy, Refractory High Entropy Alloy, High Temperature, High Pressure*

I. INTRODUCTION

For millennia, the core principle of alloying in material engineering has revolved on the technique of incorporating minute quantities of a select few secondary elements into a primary element. Nevertheless, distinct alloys made of a variety of primary elements, including aluminum, iron, since the development of nickel, copper, and zinc, the total number of alloys, the most of which have already been located and studied, is severely constrained in terms of the major element method. Thus, an innovative alloying concepts are in great demand because they greatly expand the compositional space available for the creation of new materials.

Most typical alloys consist mostly of a single principal component. In order to enhance the characteristics, various trace elements are included with the primary component, resulting in the formation of diverse alloys. However, the variety of binary alloys is limited, as periodic table has limited elements. The emergence of HEA and multi-principal element alloys (MPEA) introduced a novel approach to finding a solution. The first investigation on MPEA started in the late 1970s and subsequently evolved into a project in 1998, culminating in its publication in 2004[1]. The new notion of HEA was introduced in the same year [2]. High-entropy alloys (HEAs) exhibit distinctive characteristics due to their composition consisting of many elements. The distinctive characteristics of HEA make it attractive across several industries.

The discovery of novel materials that can withstand severe temperatures for high-temperature applications has been the primary focus of material scientists. HEAs have a distinct characteristic and attractiveness for use in structural applications under high temperatures. The material has many exceptional characteristics, such as the capacity to maintain its strength at high temperatures, excellent

stability in terms of heat, substantial toughness when exposed to very low temperatures, and outstanding resistance to wear and oxidation [3-8]. The compressor, combustor, turbine blade, and nozzle are the three primary components of the turbine engine. In recent years, the aeronautics industry has demanded novel material breakthroughs for aero-engine components that must meet thrust, weight, safety, durability, and environmental requirements Consequently, aero engines use steels, titanium alloys, nickel superalloys, aluminum alloys, and, more recently, high entropy alloys [9]. HEAs show significant promise for many structural jet engine applications.

The existing HEAs may be categorized into two groups according to their elemental makeup. One consists of transition metals for instance Co, Cr, Cu, Fe, and Ni, while the second group is based on refractory metal elements like Mo, Ti, V, Nb, Hf, Ta, Cr, and W. The concept of RHEAs came first by Senkov et al. in 2010. The researchers included refractory elements into HEAs and conducted an investigation [10]. Niobium molybdenum tantalum tungsten, also known as vanadium niobium molybdenum tantalum tungsten [11]. These two RHEAs exhibit outstanding performance at high temperatures and have melting points and elevated-temperature mechanical qualities that surpass those of conventional nickel-based superalloys. The demonstration highlights the prospective ability of RHEAs to eventually replace nickel-based superalloys as materials suitable for applications requiring high temperatures.

RHEAs have exceptional mechanical properties, including as resistance to corrosion, oxidation, and high and room temperatures [12]. Moreover, they provide a broad spectrum of prospective applications and research advantages. In recent years, there has been a more thorough and extensive research conducted on RHEAs. This paper provides a comprehensive evaluation of the scientific progress made in the field of RHEAs. This study examines the distinct characteristics of RHEAs, including their microstructure, mechanisms for strengthening, and procedures for toughening. The ductility of room temperature RHEAs is discussed. The last section offers a summary of the related RHEA problems, along with a viewpoint on potential future progress and areas of study.

II. OVERVIEW OF HIGH ENTROPY ALLOY (HEA)

2.1 Definition of HEA:

The phrase "high entropy" came from the increased configurational entropy that arises when several components are mixed together. The presence of a high configurational entropy facilitates the formation of a homogeneous solid solution (SS) [2]. Nevertheless, the study undertaken by MPEAs did not address the notion of a solitary solid solution phase propelled by entropy [1]. There are two distinct definitions that exist about HEA. One method relies on composition, while the second method relies on entropy.

2.1.1 Composition-based definition:

Yeh et al [2] offered the first description based on composition. Alloys that consist of five or more main elements are referred to as High Entropy Alloys (HEAs). The atomic composition of each primary element must fall between the range of 5 to 35 percent [2, 13]. In order to augment the quantity of high-entropy alloys (HEAs), it is possible to include minor elements, each comprising less than 5% of the total composition, together with the principal alloy. This definition does not need either the equimolar ratio or the single-phase SS.

2.1.2 Entropy-based definition:

The sum of the configurational, vibrational, magnetic dipole, and electronic randomness entropies is the total mixing entropy. Nevertheless, the configurational entropy has a greater influence on the overall mixing entropy [14, 15]. Boltzmann's equation states that a system's configurational entropy may be calculated as follows

$$\Delta S_{conf} = k \ln w \quad (1)$$

In this context, the symbol k represents Boltzmann's constant, whereas w denotes the number of possible arrangements or divisions of the system's energy among its particles. The following procedure may be used to find an equimolar alloy's configurational entropy

$$\Delta S_{conf} = - k \ln w = - R \left(\frac{1}{n} \ln \frac{1}{n} + \frac{1}{n} \ln \frac{1}{n} + \cdots + \frac{1}{n} \ln \frac{1}{n} \right) = - R \ln \frac{1}{n} = R \ln n \quad (2)$$

The entropy rises in proportion to the number of components. During the process of melting, the change in entropy per mole, represented as ΔSf, while transitioning from a solid to a liquid state, is roughly equal to one gas constant R. In a stochastic solid solution, the entropy of mixing per mole is greater, resulting in a decrease in free energy. Gibbs' law states that the decrease in free energy leads to increased stability of SS phases. Hence, the presence of configurational entropy directly affects the stability of different phases. The table below, Table 1, demonstrates the relationship between the number of elements and the corresponding rise in configurational entropies. The ternary alloy exhibits a 10% increase compared to R, whereas the quinary alloy shows a 61% increase compared to R. In their study, Yeh et al. determined a barrier of 1R to separate medium entropy alloys (MEA) from low entropy alloys and a threshold of 1.5R to identify HEAs from MEAs [16].

Table 1. Configurational entropies with different elements number [16].

N	1	2	3	4	5	6	7	8	9	10	11	12	13
ΔS_{conf}	0	0.69R	1.1R	1.39R	1.61R	1.79R	1.95R	2.08R	2.2R	2.3R	2.4R	2.49R	2.57R

The atomic bonding energy could not be overcome by mixing entropy below 1R. Fig 1 with the image is shown below.

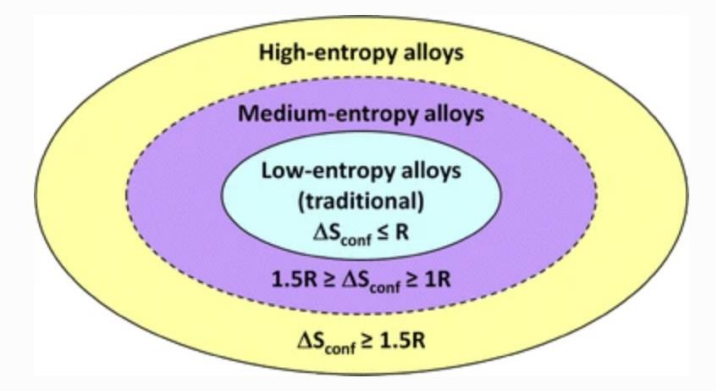

Fig 1. Different alloy based on different configurational entropy [16]

2.2 Four Core Effects:

Entropy rises in direct proportion to the number of components. During the process of melting, the change in entropy per mole, denoted as ΔS_f, while transitioning from a solid to a liquid state is roughly equal to one gas constant R. In a stochastic solid solution, the entropy of mixing per mole is elevated, leading to a decrease in the free energy. Gibbs' law asserts that phases of solid solutions become more stable as free energy decreases. Therefore, the stability of various phases is strongly impacted by the existence of configurational entropy. The table below, Table 1, illustrates the relationship between the number of elements and the corresponding rise in configurational entropies. The ternary alloy exhibits a 10% increase compared to R, whereas the quinary alloy shows a 61% increase compared to R.

2.2.1 High Entropy Effect:

The high-entropy effect states that by reducing the free energy in a HEA at high temperatures, the enhanced mixing entropy promotes the development of a solid solution phase. Furthermore, the reciprocal solubility of the elements was enhanced by this greater mixing entropy, which considerably reduced the phases in a HEA. As per Gibbs phase rules, during equilibrium condition the phase calculation is

$$P = C + 1 — D \quad (3)$$

Here, C represents the total number of elements, D represents the number of thermodynamic degrees of freedom.
As per the Gibbs free energy rules,

$$\Delta Gmix \equiv \Delta Hmix - T\Delta Smix \quad (4)$$

Here $\Delta Gmix$ represents the free energy, $\Delta Hmix$ is mixing enthalpy and $\Delta Smix$ is mixing entropy.

At high temperature phase stability is related with higher entropy. A metal melts according to Richard's rule, which says that the gas constant (R) is equal to the difference in entropy between the liquid and solid phases at the melting point. The multi principal-element design of HEAs results in a notable disparity in entropy between random solid solutions (RSS) and compounds. As an example, a high-entropy alloy (HEA) containing five distinct elements in equal proportions has a configurational entropy 1.61 times that of the gas constant (R). This implies that the entropy difference between two states of pure metals is only approximately 60% of that between an equiatomic quinary solution and a fully ordered phase. Consequently, the SS phases in HEAs are very prone to become the stable phase at high temperatures. Formation enthalpy significantly influences the phase stability. If the enthalpy of intermetallic compounds can match the large amount of entropy generated, then they can be stable at high temperatures.

2.2.2 Sluggish Diffusion Effect:
Compared to normal alloys, High-Entropy Alloys (HEAs) have slower phase transition and diffusion rates [17]. There are two perspectives on this. First, there is some diversity in the atoms around each lattice site in HEA. Consequently, the atomic motion towards an empty space is distinct. Each site exhibits distinct atomic bonding and thus, varying energies that arise from disparities in the local atomic arrangement. An atom is rendered immobile in a low-energy location, which reduces its chances of escaping. On the other hand, the atom is more likely to return to its starting location if the site exhibits significant energy. The diffusion process is hindered in any of these scenarios. Tsai et al. demonstrated the reduced mobility of Ni atoms in a quinary alloy compared to a ternary alloy and pure metal [16]. In comparison to the ternary alloy (Fe-Cr-Ni), the quinary alloy (Co-Cr–Fe–Mn–Ni) has a 50% greater energy difference across lattice sites. Furthermore, the Co–Cr–Fe–Mn–Ni alloy has a greater activation energy. Consequently, the pace at which Ni spreads is decreased.

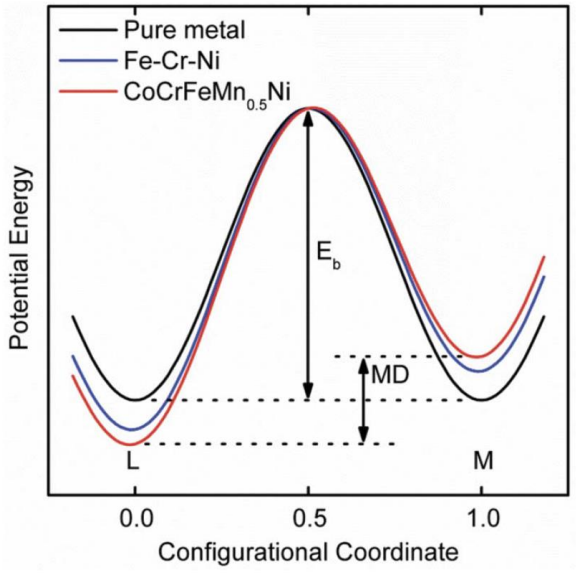

Fig 2. The potential energy changes due to the movement of Ni atoms. Here Md is the mean difference [6]

Furthermore, within a high-entropy alloy (HEA), distinct components exhibit varying rates of diffusion. Elements that are more active have a greater likelihood and opportunity to move into vacancies compared to others. However, the creation of phases is contingent upon the coordinated spread of all the constituent parts. The initiation and development of a new phase need the redistribution of all the

constituents. Additionally, for a successful migration, the cooperation of all components is required in facilitating the movement of grain borders. In this scenario, the phase change is contingent upon the parts that exhibit the slowest movement. The sluggish diffusion behavior seen in high-entropy alloys (HEAs) offers many advantages in terms of regulating phase change and characteristics [6, 18, 19], including the development of small precipitates and the creation of supersaturated states. The slow diffusion effect enhances the capacity to use high temperatures and increases the overall structural stability.

2.2.3 Severe Lattice Distortion Effect:

HEAs are compounds that bind together distinct elements with varying atomic sizes. The variation in atomic size influences the total lattice strain and stress energy. For example, the larger atom undergoes collisions with the smaller atoms, exerting a force that displaces them, while the smaller atoms possess a greater amount of free space in their vicinity. The high-entropy alloys' (HEAs) lattice structure was deformed as a result of this procedure. As a result, a high-entropy alloy's (HEA) total free energy increased.

Moreover, this lattice distortion exerts control on the characteristics of an alloy by restricting the mobility of dislocation slips. What causes an increase in solid solution hardening. Furthermore, there was an observed increase in both strength and hardness [11]. When there is significant lattice distortion, electrons and phonons scatter, which lowers thermal conductivity [20].

2.2.4 Cocktail Effect:

The qualities of a HEAs are determined by the characteristics of each of its constituent elements. This approach facilitates the selection of materials depending on their qualities in order to create a specific alloy. For example, the inclusion of any lightweight element will result in a reduction in the overall density of an alloy. Both the individual pieces and their interrelation are equally crucial. Fig 3 shows how adding additional aluminum causes the phase to shift from face-centered cubic (FCC) to body-centered cubic (BCC), which increases the alloy's hardness and decreases its ductility. Al develops a strong cohesive bond with other elements.

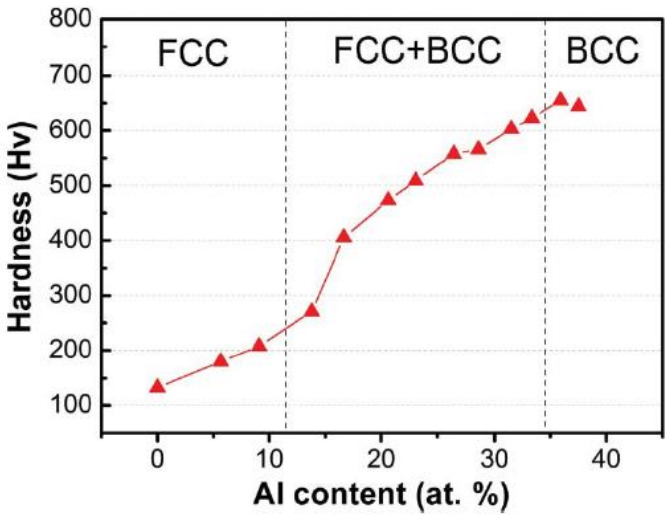

Fig 3: Hardness of $Al_xCoCrCuFeNi$ increases with increasing Al

III. HIGH ENTROPY ALLOY AT HIGH PRESSURE

3.1 Microstructure of HEA at High Pressure:

In last one and half decades, numerous research on HEA happened in order to develop different HEAs which holds unique material properties. Moreover, searching new materials which can stand it's properties at extreme conditions. Tsai and Yeh [1] first categorized the phases based on hardness in table 2.

Table 2: Categorized the phases based on hardness [21]

Type	Examples	Typical hardness [HV]
Valence compounds	Carbides, borides, silicides	1000–4000
IM phases with non-simple structures	σ, Laves, η	650–1300
BCC and derivatives	BCC, B2, Heusler	300–700
FCC and derivatives	FCC, L12, L10	100–300

with it's properties under extreme conditions (high pressures) is the necessity in the material science field. To fabricate such HEA, we need to know the microstructure of those HEAs. The microstructure of a HEA plays a crucial role in determining its characteristics.

3.1.1 Face centered cubic (FCC) Structure:

The FCC structured HEAs have low levels of hardness and yield strength, while demonstrating favorable qualities of ductility and strain hardening capabilities. The Cantor alloy, composed of CoCrFeMnNi, has been extensively researched as a high-entropy alloy (HEA) and has shown exceptional structural stability over several temperature ranges. On the contrary, the Cantor alloy underwent a phase shift from face-centered cubic (fcc) to body-centered cubic (bcc) or hexagonal close-packed (hcp) structures when subjected to high pressure [22-26]. Zhang and Wu et al. [22] demonstrated the occurrence of a polymorphic change from fcc to hcp structure in CoCrFeMnNi under conditions of high pressure and temperature. The formation of a new hcp phase starts at pressures of 22 GPa and persists until 41 GPa, during which both fcc and hcp phases coexist. The transition is characterized by a slow and irreversible process [22]. Fig 4 shows the coexistence of hcp and fcc structures during decompression till reaching the ambient pressure.

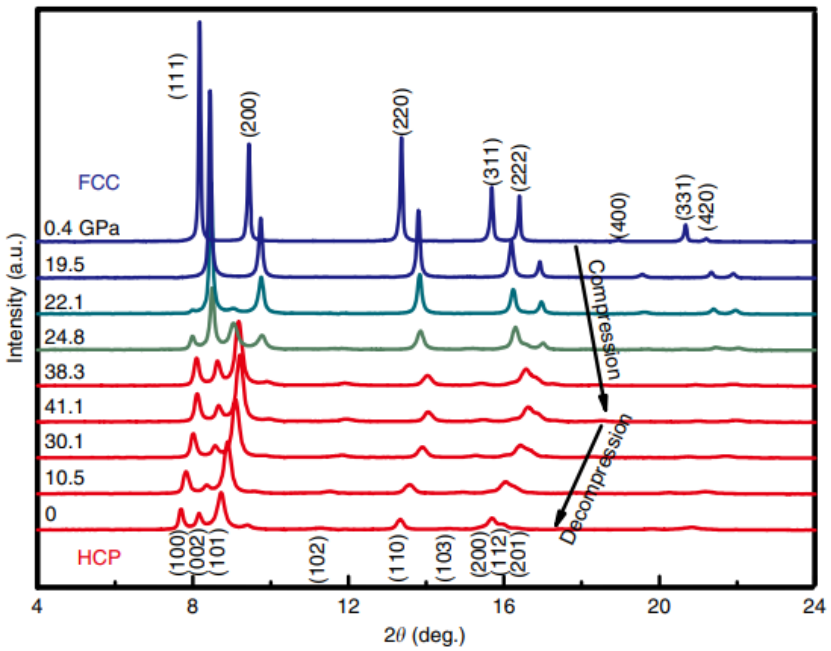

Fig 4: Shows the XRD result of Cantor alloy. The decompression and compression shows the both the phase exist at different pressure. [27]

The CoCrFeMnNi HEA undergoes a polymorphic phase change from fcc to hcp. This transition has been independently observed by many researchers within a pressure range of around 7 GPa to 49 GPa [24-26].

Zhang et al. [24] provided a clear explanation of how non-hydrostaticity and grain size impact the pressure-induced phase transition of Cantor alloy. He conducted in-situ high-pressure XRD analysis on the CoCrFeMnNi HEA samples using several non-hydrostatic pressure mediums, including Helium, Silicon Oil, and Amorphous Boron. Fig 5 demonstrates that the shift from face-centered cubic (fcc) to hexagonal close-packed (hcp) structure takes place at an initial pressure of around 22 GPa in helium,

around 7 GPa in silicon oil, and roughly between 2 to 6 GPa in amorphous boron. In order to demonstrate the grain effect, he introduced cantor alloy samples with two distinct grain sizes, one measuring around 5 μm and the other measuring 10 nm. Both materials are produced using the processes of gas atomization and high-pressure torsion (HPT) respectively showed in fig 6.

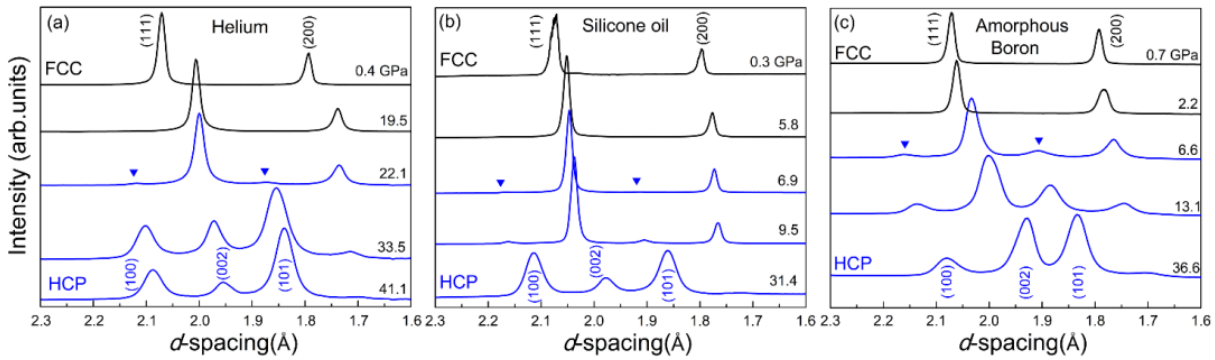

Fig 5: The XRD patterns of the CoCrFeMnNi HEA samples were obtained during compression using helium (a), silicone oil (b), and amorphous boron (c) as the pressure media [28].

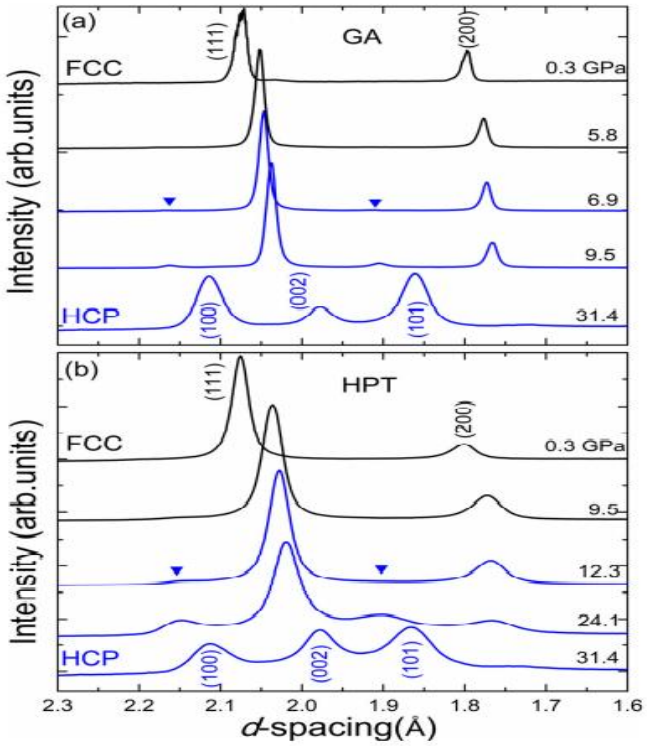

Fig 6: XRD pattern of Cantor alloy with two different grain size (a)5 μm (GA) (b) 10nm (HPT) [29].

However, the phase shift is not occurring in the homogenized Cantor alloy. Shahmir et al. [30] subjected CoCrFeNiMn HEA to HPT at ambient temperature, applying a pressure of 6 GPa. Post-deformation annealing is used to achieve an optimal balance between ductility and strength. The hardness was shown to rise up to a temperature of 773K as a result of the creation of the brittle σ phase. Table 3 demonstrates that subjecting the material to annealing at a temperature of 1073K for a duration of 10 minutes resulted in the optimal balance between ultimate tensile strength and ductility. This was achieved by impeding the development of grains and dissolving precipitates. The introduction of a little amount of HEA has a substantial impact on both the microstructure and characteristics. Yusenko et al. [31] substituted manganese in the cantor alloy with a little amount of aluminium and produced an Al0.3CoCrFeNi HEA via vacuum arc melting. This alloy maintains a fcc structure at a compressive pressure of 60 GPa at ambient temperature. However, refraining grain by thermal

Table 3: Mechanical properties of CoCrFeNiMn HEA before and after PDA from 1073-1173 K. [30]

Annealing temperature (K)	Annealing time (min)	Hv	YS (MPa)	UTS (MPa)	δ (%)
Homogenized		120	300	530	85
1073	10	290	680	830`	65
1073	30	245	570	725	78
1073	60	220	530	680	80
1173	10	170	410	630	76
1173	30	155	390	610	80
1173	60	140	370	600	90

annealing may lead to change the microstructure. $Al_{0.3}CoCrFeNi$ manufactured via high pressure torsion formed fcc. During post annealing, ordered bcc structure observed at 663K temperature [23]. Fig 7 displays the XRD pattern of the $Al_{0.3}CoCrFeNi$ HEA after undergoing thermal annealing, transitioning from a nanocrystalline state at room temperature (NC-RT) to a nanocrystalline state at 973K (NC-973K). BCC phase appeared from 663K.

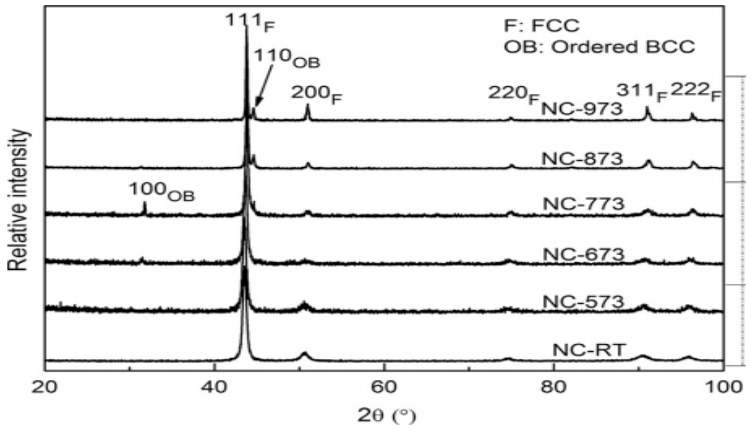

Fig 7. XRD pattern of $Al_{0.3}CoCrFeNi$ HEA with post annealing [32]

The occurrence of phase change is contingent upon the various kinds of grains present. Sathiyamoorthi et al [33] produced $Fe_{40}Mn_{40}Co_{10}Cr_{10}$ using the process of high-pressure torsion. The disc was subjected to annealing and then compressed to a pressure of 4 gigapascals (GPa). Both fine-grained and coarse-grained samples are used. The phase underwent a partial transformation from fcc to hcp and bcc. A higher occurrence of bcc phase was reported in the coarse grain sample compared to the fine grain sample [33]. Extreme pressure causes deformation and transformation of phases within an alloy. At ambient temperature, the $Mo_{7.5}Fe_{55}Co_{18}Cr_{12.5}Ni_7$ medium entropy alloy undergoes a transition from a fcc structure to a bcc structure as a result of deformation [34].

3.1.2 Body Centered Cubic Structure:

The BCC phase is highly sought after in the nuclear plant, jet engine, and aerospace industries because to its exceptional hardness and thermal stability. It has greater resilience to deformation. Hence, it is crucial to examine the phase stability and transition of bcc structure. The introduction of Al content into the CoCrFeNi alloy results in a phase transition from a fcc structure to a combination of fcc and bcc structures, eventually leading to a full bcc structure [2, 35, 36]. Aluminium, due to its greater atomic size compared to the other four elements, generated lattice deformation, resulting in a more stable phase [35, 37]. Li et al. conducted a study to investigate the phase stability of the bcc + fcc AlCoCrCuFeNi HEA under high compressive pressure at ambient temperature. The HEA maintains its fcc and bcc phases at pressures of up to 24 GPa [38]. Fig 8 demonstrates that there is no change in phase, and the peaks stay consistent under varying pressure conditions. This distinctive attribute prompted further investigation into the phase stability in conditions of high pressure and temperature. The inclusion of trace elements to induce precipitation is a crucial factor in shaping the microstructure of an alloy [39-41]. Yusenko et al. investigated the phase stability of $Al_2CoCrFeNi$ HEA at high pressure and

temperature settings, with and without the inclusion of 3 atomic percent scandium [31]. Scandium has excellent thermal stability when combined with the majority of high-entropy alloy constituents. The stability of bcc structured $Al_2CoCrFeNi$, both with and without Sc, was observed up to a compressive pressure of 60 GPa at ambient temperature. Nevertheless, the addition of 3 atomic percent Sc to $Al_2CoCrFeNi$ resulted in the formation of hexagonal intermetallic phases at the grain boundaries. These phases provided the material with the ability to endure high temperatures and pressures.

Cheng et al. [42] examined the polymorphic transitions of bcc structured AlCoCrFeNi HEA caused by pressure. The researcher used in situ synchrotron radiation XRD to compress the sample to a pressure of 42 GPa, and then decompressed it back to ambient pressure. Fig 9 of the XRD analysis demonstrates the stability of the B2 phase at a pressure of 17.6 GPa. The (100), (200), and (111) peaks vanish at increased pressure. While the peak at (110) remains robust. This indicates that a phase change occurred at a pressure over 17.6 GPa. During the process of decompression, all peaks regain their original intensity and width, with the exception of the (111) peak. The peak maintains its breadth and intensity at (111). By analyzing both the in situ XRD and ex situ transmission electron microscopy (TEM), it has been shown that the significant deformation of the crystal lattice is associated with the phase transition.

To have a more profound comprehension of polymorphism in the bcc structure, Wang et al. conducted an analysis of the phase change of $Al_{0.6}CoCrFeNi$ HEA using in situ synchrotron radiation XRD [43]. The phase change from the initial bcc phase to the orthorhombic phase begins at a compressive pressure of 10 GPa. This novel phase exhibits stability up to 40 gigapascals (GPa). The intense pressure resulted in significant lattice strain inside the structure. By removing all lattice tensions, the change from the orthorhombic phase to the body-centered tetragonal phase (BCT) occurs. Fig 10 shows the emergence of a novel peak at a pressure of 10.6 GPa, indicating the beginning of a phase transition. At a pressure of 21.4 gigapascals, the original peak completely disappeared. The phase change has concluded.

In contrast with the above transformation, when the initial bcc structured $Al_{0.6}CoCrFeNi$ annealed at 1000^0C for 2h then bcc changed to stable fcc phase. With the extreme pressure this fcc phase transformed to hcp structure. In this study, total five polymorphs found from ambient condition to extreme condition.

To have a more profound comprehension of lattice strain when subjected to compressive stress, Reiberg et al. created two multi principal elemental alloys (MPEA) consisting of aluminium, chromium, iron, nickel, and titanium, along with some other minor elements [44]. MPEA5 has an equimolar ratio with Al, Cr, Fe, Ni, and Ti. Additionally, there is a variant with a decreased titanium content of up to 10%, known as MPEA_Ti10. Under conditions of elevated temperature and pressure, the alloy exhibited three distinct phases: bcc, complete Heusler, and C14_Laves. By decreasing the amount of titanium, MPEA_Ti10 exhibited a decrease in the presence of C14_leaves phases. The presence of fewer C14_leaves phases in MPEA_Ti10 led to enhanced resistance against the formation of extensive fractures. Extensive fractures appeared in MPEA5 over time. The presence of these fissures influenced the stress-strain characteristics of MPEA5 and MPEA_Ti10.

Studying the transition from a dual or multi-phase state to a single phase is a fascinating area of research. Liu et al. observed a phase change in $AlCrFe_2Ni_2$ when subjected to HPT at a compressive pressure of 6 Gpa. The transition included a change from a fcc structure to an ordered B2 structure, and then to a bcc structure, before finally returning to the original fcc structure [46]. The application of torsional strain altered the diffusion behavior, leading to the occurrence of a phase transition. RHEA are a novel category of materials that possess a high melting temperature, allowing them to be used under harsh environments. Ahmad et al. conducted a study on $Hf_{25}Nb_{25}Zr_{25}Ti_{25}$ RHEA at high pressure and temperature and observed phase stability [26]. This thermally and mechanically robust HEA may be used in very demanding conditions characterized by elevated temperatures and pressures. Zhange et al. conducted research on a dual-phase The TiZrHfNb HEA exhibits an outstanding lattice distortion of up to 2.39% [47], surpassing that of other HEAs.

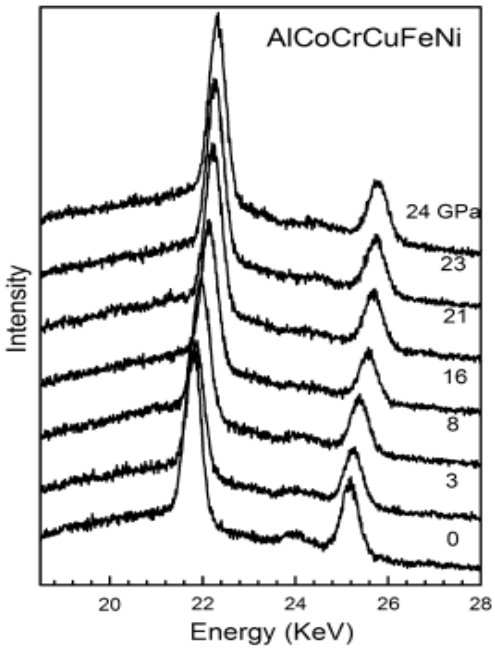

Fig 8. In situ XRD of AlCoCrCuFeNi with synchrotron radiation [45]

The first TiZrHfNb HEA has a dual-phase composition characterized by a body-centered cubic structure. Fig 11 demonstrates that when pressure rises during compression, the minor phase steadily decreases and eventually disappears completely at 30.3 GPa. Afterwards, the monophasic state achieved a stable condition at a pressure of 67.6 gigapascals (GPa). Throughout the decompression process, the bcc structure maintained its single-phase state without any alterations. Guo et al. examined the structural integrity of the $(TaNb)_{0.67}(HfZrTi)_{0.33}$ superconducting RHEA at pressures of up to 190 GPa [48]. The bcc structure of this RHEA material stays unaltered at pressures up to 100 gigapascals (GPa).

3.1.3 Hexagonal Closed Pack Structure:

Ahmad et al examined the structural soundness of the $Re_{25}Ru_{25}Co_{25}Fe_{25}$ HEA at pressures reaching 80.4 GPa [26] (see fig 12). The HCP structured HEA maintained its stability and did not exhibit any phase shift. Certain rare earth minerals exhibit a hcp structure in HEA. Liu et al. conducted experiments on HoDyYGdTb HEA subjected to compression pressures of up to 60.1 GPa [49]. Four polymorphs were discovered. The shift from hcp to samarium type (Sm) began at a pressure of 4.4 GPa, as seen in fig 13. The second conversion from Sm to double hcp (dhcp) occurred at a pressure of 26.7 GPa. The ultimate transition occurred at a pressure of 40.2 GPa, transforming from a dhcp crystal structure to a disordered fcc crystal structure.

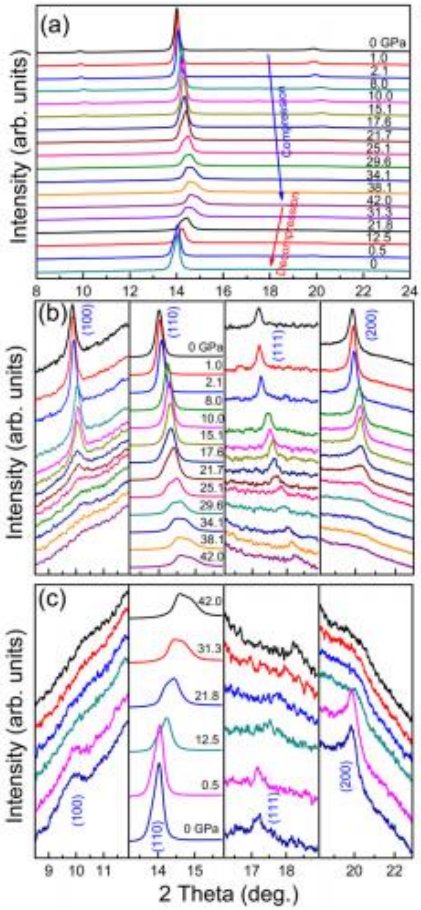

Fig 9. In situ XRD graph of AlCoCrFeNi HEA. (a) the total graph. (b) During compression and (c) During decompression [36].

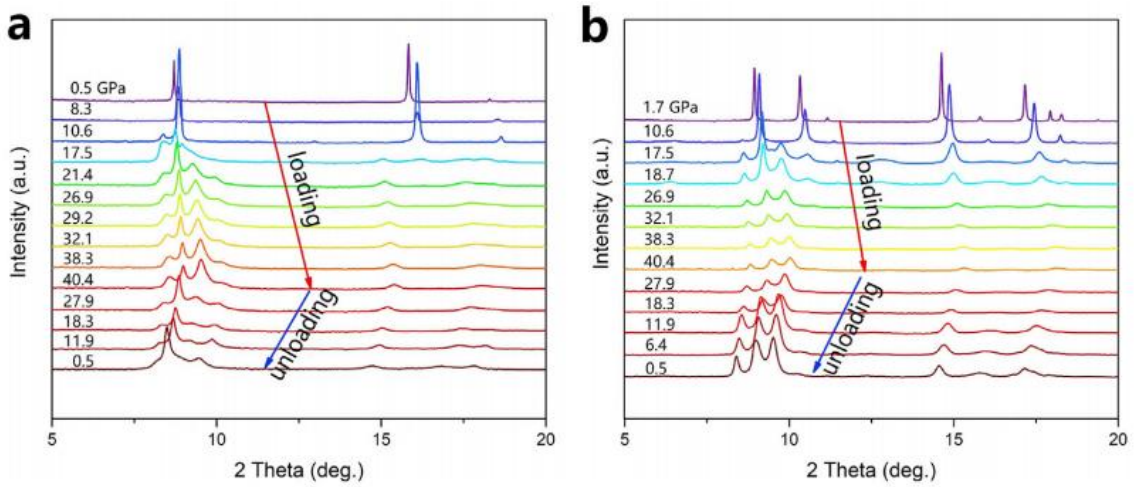

Fig 10. The in-situ synchrotron radiation XRD of $Al_{0.6}CoCrFeNi$. (a) The loading and unloading of initial BCC phase (b) The annealed $Al_{0.6}CoCrFeNi$ with FCC phase [37].

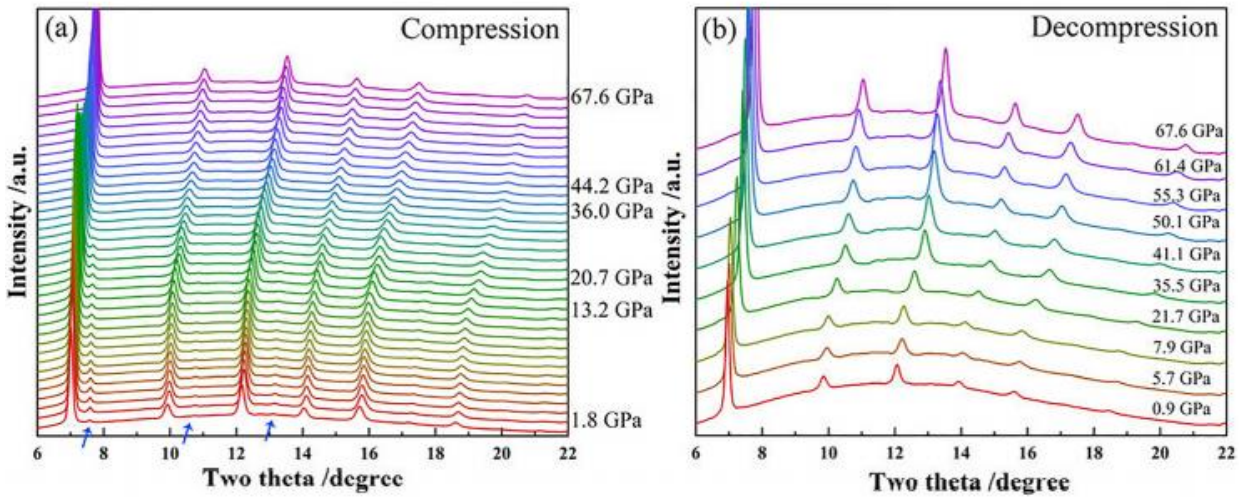

Fig 11. The XRD pattern of TiZrHfNb HEA (a) During compression (b) Decompression [43]

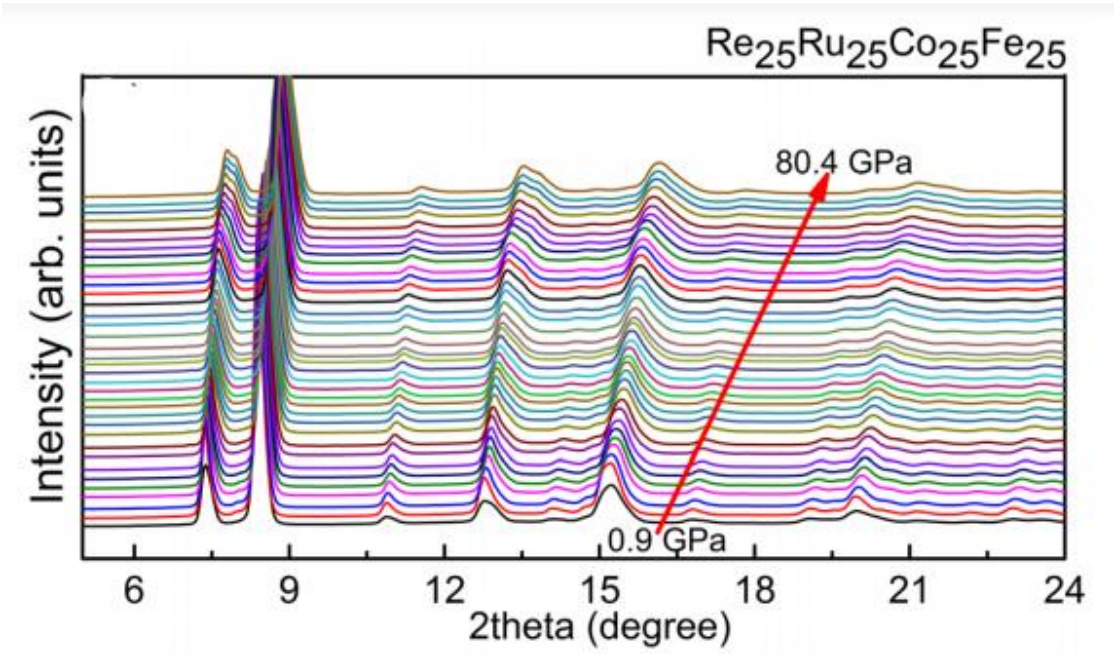

Fig 12. XRD pattern of $Re_{25}Ru_{25}Co_{25}Fe_{25}$ HEA during compression [44].

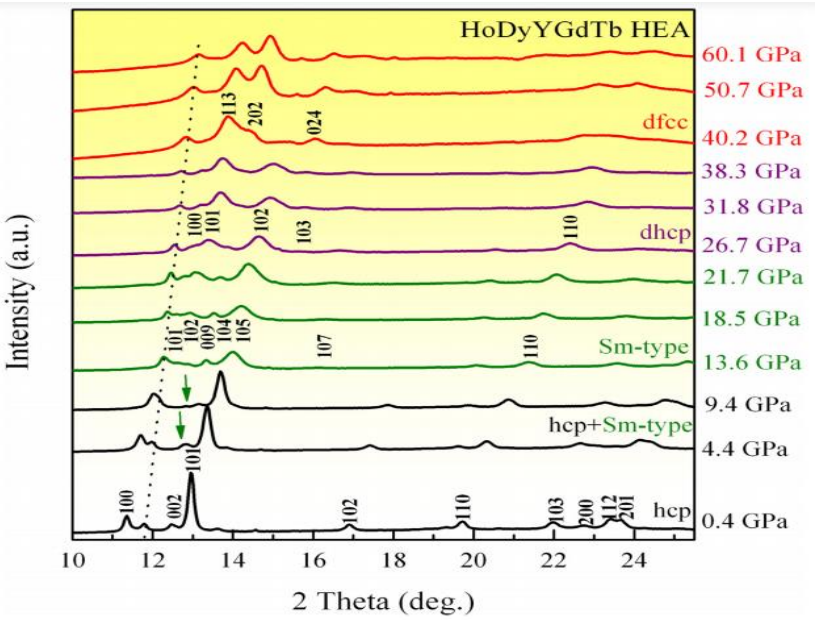

Fig 13. XRD pattern of HoDyYGdTb HEA under compression at room temperature. [43]

IV. HIGH ENTROPY ALLOY AT HIGH TEMPERATURE

4.1 Microstructure of HEA at High Temperature:

Generally, RHEAs are regarded as futuristic materials that surpass Ni-based superalloys in terms of high-temperature structural applications. Efforts should priorities the creation of RHEAs with exceptional mechanical qualities, such as high strength, ductility, and toughness. The mechanical behavior is significantly connected with the phase content, microstructure(s), and alloy composition. The composition of RHEAs suggests that the bcc phase is likely to be prevalent in these alloys. The composition of these alloys is mostly comprised of refractory metals from subgroups V and VI, which inherently have bcc crystal structures and demonstrate substantial solubility with each other. In addition, metals belonging to subgroup IV, namely titanium, zirconium, and hafnium, exhibit a bcc crystal structure at high temperatures. However, at normal temperature, they undergo an allotropic change and adopt a hcp structure. Aluminium (Al) is present in 46 RHEAs and has a fcc crystal structure. Nevertheless, it functions as a stabilizing element in the bcc structure for titanium (Ti), zirconium (Zr), and hafnium (Hf). In addition, aluminium has notable solubility in refractory metals [50, 51]. The Laves phase, also known as C14 or C15, is seen with high frequency in the reported RHEAs at high temperatures. The presence of chromium (Cr) [52-54], molybdenum (Mo), and zirconium (Zr)[31], either alone or in combination with aluminum (Al) and vanadium (V), and zirconium (Zr) is consistently seen in this context. The Laves phase exhibits stability at temperatures below the solidus in binary systems of Cr-Zr, Mo-Zr, V-Zr, and Cr-Ti, as well as in ternary systems of Mo-V-Zr and Cr-V-Zr. This stability is seen for compositions that surpass the maximum solubility of (Mo,V) or (Cr,V) in Zr, and Zr in Cr, Mo, or V [50, 51]. The presence of the laves phase in a bcc matrix may vary depending on the volume fraction and heat treatment.

The B2 phase, known for its orderly structure, has been recognized as the third most often occurring phase in recorded RHEAs. A matrix phase has been seen in 12 multiphase alloys. The alloys were either in their original cast state or exposed to both the cast state and annealing conditions at a temperature of 1200 °C. The alloys being considered have common elements, namely aluminum (Al), niobium (Nb), titanium (Ti), and zirconium (Zr). Some samples also include the elements Molybdenum (Mo), Tantalum (Ta), and/or Vanadium (V). The additional phases seen in this research include of bcc, AlxZr5, and Laves phases. The modified nanophase b2/bcc structure has a similarity to the structure seen in superalloys. Moreover, it showcases desirable attributes such as exceptional thermal stability and the ability to maintain significant amounts of strength at extreme temperatures. Refractory high entropy superalloys, which contain the B2/bcc (or bcc/B2) nanostructure, have been categorized as a new kind of RHEAs [55, 56] because they possess both common features and unique properties.

Although the B2 and bcc phases have similar lattice properties, their chemical compositions vary significantly. The bcc phase undergoes a reduction in quantity, whereas the B2 phase has an elevated level of aluminum and zirconium. The observed B2 ordering is postulated to result from the substantial interatomic interactions between aluminum (Al) and zirconium (Zr) atoms, especially in the presence of other refractory elements [55, 56].

4.2 Mechanical Properties of HEA at High Temperature:

Presently, the use of the nickel-based superalloy Inconel 718 is widespread in the field of superalloys. However, it is crucial to ensure that the temperature of this specific superalloy does not exceed 1300 °C. RHEAs provide superior high-temperature performance, which is more visually appealing. An instance of a VNbTiTaSi alloy, specifically denoted as [57] RHEA, exhibits the development of nanoscale silicide precipitates under conditions of high temperature deformation. The material has a yield strength of 505 MPa when subjected to a temperature of 1000 °C. Additionally, it demonstrates satisfactory toughness at room temperature, as seen by a ductility of 34%. In a recent study conducted by Nie et al. [58] the mechanical characteristics of HfMoScTaZr RHEA were assessed. The RHEA displayed a single disordered bcc solid solution structure. The testing results demonstrate that the Vickers microhardness and yield strength of the RHEA material are determined to be 9400 MPa and 1778 MPa, respectively. The alloy exhibits compressive yield strengths of 963 MPa and 498 MPa at temperatures of 1000 °C and 1200 °C, respectively. Xiang et al. [59] performed a study on the mechanical characteristics of a set of TaNbVTiAlx RHEAs at high temperatures. The results suggest that all TaNbVTiAlx RHEAs have a unique BCC solid solution structure, showing impressive strength at high temperatures and a reasonable amount of flexibility, as seen in Figure 8. Moreover, it is important to mention that these RHEAs have significant potential for applications, even at high temperatures of 1200 °C. To increase the heat resistance of the alloy system while maintaining sufficient toughness at normal temperatures. In their study, Juan et al. [60] made modifications to the composition of HfNbTaTizr, resulting in the creation of two novel single-phase RHEAs, namely HfMoTaTiZr and HfMoNbTaTiZr. The improved alloy exhibits a much greater yield strength in comparison to the HfNbTaTiZr alloy. When the temperature reaches 1200°C, the HfMoNbTaTiZr alloy exhibits a yield strength that is almost six times more than that of the HfNbTaTiZr alloy. The alloy demonstrated satisfactory ductility under ambient conditions. The high-temperature strengths of NbTaTiV and CrMoNbV alloys [61] are maintained by edge dislocations, as seen in fig 14. This contrasts with the screw dislocations observed in prior bcc alloys, which govern plastic flow. This work introduces novel concepts for the advancement of new RHEAs.

In the realm of RHEAs, there exists a notable inclination for elements, even those with slightly varying thermodynamic characteristics in their respective oxides, to exhibit a strong preference for oxidation. This preference may cause the material to become unstable or form solid solutions, resulting in changes to the overall characteristics of the material [62]. This study presents an analysis of the oxidation behavior of the RHEA alloy, TaMoCrTiAl, at elevated temperatures. At temperatures of 1000 and 1100 °C, the alloy exhibits the formation of thin and dense layers that are rich in aluminum. These layers demonstrate a favorable resistance to oxidation, as shown in reference [63]. In order to improve the RHEA's resistance to oxidation, Gorr et al. [64] used an innovative method by applying a CrTaO4 oxide coating over the TaMoCrTiAl HEA. The results suggest that the oxide is stable throughout a wide range of temperatures, ranging from 500°C to 1500°C. Additionally, it demonstrates ease of formation, exceptional adhesion, and a minimal growth rate during the cooling process. The evaluation of the oxidation resistance of the MoTaTiCr high-entropy alloy (HEA) demonstrated that the primary factor contributing to its exceptional oxidation resistance is the development of a continuous composite oxide layer composed of $CrTaO_4$ [64] The $NiSi_{0.5}CrCoMoNb_{0.75}$ RHEA coating was successfully synthesized by Li et al. demonstrating good resistance to oxidation at elevated temperatures.

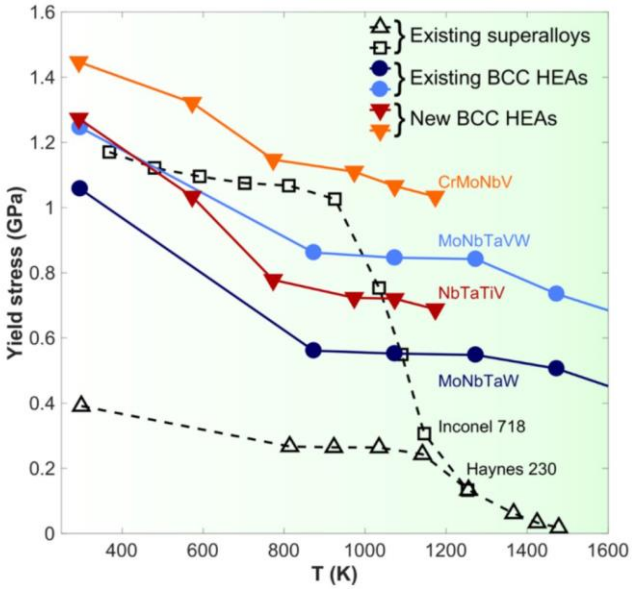

Fig 14: The refractory bcc HEAs exhibit exceptional strength retention at elevated temperatures, surpassing the temperature thresholds at which superalloys typically experience strength degradation. The NbTaTiV alloy examined in this study has similar characteristics to the MoNbTaV and MoNbTaW alloys documented in the existing literature. The CrMoNbV alloy exhibits a notable increase in strength, surpassing the strengths of the current body-centered cubic (HEAs. The dominant factor influencing the mechanical properties of NbTaTiV and CrMoNbV alloys is mostly due to edge dislocations, rather than screw dislocations [61].

V. CONCLUSIONS

HEAs is emerging due to it's excellent material properties at extreme conditions. The world is limited with the elements. In order to expand this field, there is no alternative than to alloying multiple elements and observing their results through different processes. Therefore, understanding this alloy's nature, core effects, microstructure and mechanical properties at high temperature and pressure is important.

HEA can be defined either based on entropy or based on composition. Four fundamental core effects dictate the properties of the alloy. Mixing multiple elements together increases the entropy and decrease multiples phases. The diffusion rate of each element connected with the phase formation. In HEAs, the new lattice distorted by the different atoms and block the dislocation slip's movement. As a result, the mechanical properties improve.

Microstructure of a HEAs can be changed at high pressure. Cantor alloy transformed from fcc to hcp when the pressure is more than 41GPa. Non-hydrostaticity and grain size affects the phase transition. Minor addition of an element with the alloy also significantly impacts the phase transition at high pressure.

RHEA has significant impact in high temperature application due to it's superior mechanical properties and high melting point. Most RHEA possess bcc phase at high temperature. However, some other leaves phases, B2 and hcp phases also shown.

Ni super alloy can't sustain it's mechanical properties beyond 1300^0C. To support that gap, RHEA is a promising material. RHEA can sustain its strength and oxidation resistance at elevated temperature beyond 1300^0C.

REFERENCES

[1]. Cantor, B., et al., *Microstructural development in equiatomic multicomponent alloys.* Materials Science and Engineering: A, 2004. **375**: p. 213-218.

[2]. Yeh, J.W., et al., *Nanostructured high-entropy alloys with multiple principal elements: novel alloy design concepts and outcomes.* Advanced engineering materials, 2004. **6**(5): p. 299-303.

[3]. Huang, P.K., et al., *Multi-principal-element alloys with improved oxidation and wear resistance for thermal spray coating.* Advanced Engineering Materials, 2004. **6**(1-2): p. 74-78.

[4]. Miracle, D.B., et al., *Exploration and development of high entropy alloys for structural applications.* Entropy, 2014. **16**(1): p. 494-525.

[5]. Pickering, E. and N. Jones, *High-entropy alloys: a critical assessment of their founding principles and future prospects.* International Materials Reviews, 2016. **61**(3): p. 183-202.
[6]. Senkov, O., et al., *Oxidation behavior of a refractory NbCrMo 0.5 Ta 0.5 TiZr alloy*. Journal of Materials Science, 2012. **47**: p. 6522-6534.
[7]. Cheng, C.-Y. and J.-W. Yeh, *High thermal stability of the amorphous structure of GexNbTaTiZr (x= 0.5, 1) high-entropy alloys.* Materials Letters, 2016. **181**: p. 223-226.
[8]. Miracle, D.B. and O.N. Senkov, *A critical review of high entropy alloys and related concepts.* Acta Materialia, 2017. **122**: p. 448-511.
[9]. Alderliesten, R., *Introduction to aerospace structures and materials*. 2018: Delft University of Technology.
[10]. Senkov, O., et al., *Refractory high-entropy alloys.* Intermetallics, 2010. **18**(9): p. 1758-1765.
[11]. Senkov, O.N., et al., *Mechanical properties of Nb25Mo25Ta25W25 and V20Nb20Mo20Ta20W20 refractory high entropy alloys.* Intermetallics, 2011. **19**(5): p. 698-706.
[12]. Gao, M.C., et al., *Senary refractory high-entropy alloy HfNbTaTiVZr*. Metallurgical and Materials Transactions A, 2016. **47**: p. 3333-3345.
[13]. Jien-Wei, Y., *Recent progress in high entropy alloys.* Ann. Chim. Sci. Mat, 2006. **31**(6): p. 633-648.
[14]. Fultz, B., *Vibrational thermodynamics of materials.* Progress in Materials Science, 2010. **55**(4): p. 247-352.
[15]. Swalin, R.A. and J. Arents, *Thermodynamics of solids.* Journal of The Electrochemical Society, 1962. **109**(12): p. 308C.
[16]. Yeh, J.-W., *Alloy design strategies and future trends in high-entropy alloys.* Jom, 2013. **65**: p. 1759-1771.
[17]. Cheng, K.-H., et al. *Recent progress in multi-element alloy and nitride coatings sputtered from high-entropy alloy targets*. in *Annales de chimie (Paris. 1914)*. 2006.
[18]. Kao, Y.-F., et al., *Microstructure and mechanical property of as-cast,-homogenized, and-deformed AlxCoCrFeNi (0≤ x≤ 2) high-entropy alloys.* Journal of Alloys and Compounds, 2009. **488**(1): p. 57-64.
[19]. Cheng, C.-Y. and J.-W. Yeh, *High-entropy BNbTaTiZr thin film with excellent thermal stability of amorphous structure and its electrical properties.* Materials Letters, 2016. **185**: p. 456-459.
[20]. Kao, Y.-F., et al., *Electrical, magnetic, and Hall properties of AlxCoCrFeNi high-entropy alloys.* Journal of alloys and compounds, 2011. **509**(5): p. 1607-1614.
[21]. Perepezko, J.H., *The hotter the engine, the better.* Science, 2009. **326**(5956): p. 1068-1069.
[22]. Zhang, F., et al., *Polymorphism in a high-entropy alloy.* Nature communications, 2017. **8**(1): p. 15687.
[23]. Tracy, C.L., et al., *High pressure synthesis of a hexagonal close-packed phase of the high-entropy alloy CrMnFeCoNi.* Nature communications, 2017. **8**(1): p. 15634.
[24]. Zhang, F., et al., *Effects of non-hydrostaticity and grain size on the pressure-induced phase transition of the CoCrFeMnNi high-entropy alloy.* Journal of Applied Physics, 2018. **124**(11).
[25]. Huang, E.-W., et al., *Irreversible phase transformation in a CoCrFeMnNi high entropy alloy under hydrostatic compression.* Materials Today Communications, 2018. **14**: p. 10-14.
[26]. Ahmad, A.S., et al., *Structural stability of high entropy alloys under pressure and temperature.* Journal of Applied Physics, 2017. **121**(23).
[27]. Wang, W., et al., *Role of Re and Co on microstructures and γ′ coarsening in single crystal superalloys.* Materials Science and Engineering: A, 2008. **479**(1-2): p. 148-156.
[28]. Tian, S.-G., et al., *Microstructure evolution and deformation features of single crystal nickel-based superalloy containing 4.2% Re during creep.* Transactions of Nonferrous Metals Society of China, 2011. **21**(7): p. 1532-1537.
[29]. Kaciulis, S., et al., *Relation between the microstructure and microchemistry in Ni-based superalloy.* Surface and interface analysis, 2012. **44**(8): p. 982-985.
[30]. Shahmir, H., et al., *Effect of annealing on mechanical properties of a nanocrystalline CoCrFeNiMn high-entropy alloy processed by high-pressure torsion.* Materials Science and Engineering: A, 2016. **676**: p. 294-303.
[31]. Yusenko, K.V., et al., *High-pressure high-temperature tailoring of high entropy alloys for extreme environments.* Journal of Alloys and Compounds, 2018. **738**: p. 491-500.
[32]. Tang, Q., et al., *Hardening of an Al0. 3CoCrFeNi high entropy alloy via high-pressure torsion and thermal annealing.* Materials letters, 2015. **151**: p. 126-129.
[33]. Sathiyamoorthi, P., et al., *Unusual strain-induced martensite and absence of conventional grain refinement in twinning induced plasticity high-entropy alloy processed by high-pressure torsion.* Materials Science and Engineering: A, 2021. **803**: p. 140570.
[34]. Nguyen, N.T.-C., et al., *Superplastic Behavior in High-Pressure Torsion-Processed Mo 7.5 Fe 55 Co 18 Cr 12.5 Ni 7 Medium-Entropy Alloy.* Metallurgical and Materials Transactions A, 2021. **52**: p. 1-7.

[35]. Zhang, Y., et al., *Microstructures and properties of high-entropy alloys.* Progress in materials science, 2014. **61**: p. 1-93.
[36]. Sheng, G. and C.T. Liu, *Phase stability in high entropy alloys: Formation of solid-solution phase or amorphous phase.* Progress in Natural Science: Materials International, 2011. **21**(6): p. 433-446.
[37]. Miyamoto, G., et al., *Effects of Mn, Si and Cr addition on reverse transformation at 1073 K from spheroidized cementite structure in Fe–0.6 mass% C alloy.* Acta Materialia, 2010. **58**(13): p. 4492-4502.
[38]. Li, G., et al., *Equation of state of an AlCoCrCuFeNi high-entropy alloy.* Jom, 2015. **67**: p. 2310-2313.
[39]. Chuang, M.-H., et al., *Microstructure and wear behavior of AlxCo1. 5CrFeNi1. 5Tiy high-entropy alloys.* Acta Materialia, 2011. **59**(16): p. 6308-6317.
[40]. Singh, S., et al., *Decomposition in multi-component AlCoCrCuFeNi high-entropy alloy.* Acta Materialia, 2011. **59**(1): p. 182-190.
[41]. Chuang, M.-H., et al., *Intrinsic surface hardening and precipitation kinetics of Al0. 3CrFe1. 5MnNi0. 5 multi-component alloy.* Journal of alloys and compounds, 2013. **551**: p. 12-18.
[42]. Cheng, B., et al., *Pressure-induced phase transition in the AlCoCrFeNi high-entropy alloy.* Scripta Materialia, 2019. **161**: p. 88-92.
[43]. Wang, L., et al., *Abundant polymorphic transitions in the Al0. 6CoCrFeNi high-entropy alloy.* Materials Today Physics, 2019. **8**: p. 1-9.
[44]. Reiberg, M., et al., *Lattice strain during compressive loading of AlCrFeNiTi multi-principal element alloys.* Continuum Mechanics and Thermodynamics, 2021. **33**: p. 1541-1554.
[45]. Li, G., et al., *Equation of state of an AlCoCrCuFeNi high-entropy alloy.* Jom, 2015. **67**(10): p. 2310-2313.
[46]. Liu, X., et al., *Evidence for a phase transition in an AlCrFe2Ni2 high entropy alloy processed by high-pressure torsion.* Journal of Alloys and Compounds, 2021. **867**: p. 159063.
[47]. Zhang, K., et al., *Tuning to more compressible phase in TiZrHfNb high entropy alloy by pressure.* Applied Physics Letters, 2020. **116**(3).
[48]. Guo, J., et al., *Robust zero resistance in a superconducting high-entropy alloy at pressures up to 190 GPa.* Proceedings of the National Academy of Sciences, 2017. **114**(50): p. 13144-13147.
[49]. Yu, P., et al., *Pressure-induced phase transitions in HoDyYGdTb high-entropy alloy.* Materials Letters, 2017. **196**: p. 137-140.
[50]. Thaddeus, B.M., *Binary alloy phase diagrams second edition.* Materials Park Ohio, 1990: p. 2705-2708.
[51]. Villars, P., *Handbook of ternary alloy phase diagrams.* ASM international, 1995. **7**: p. 8754-8755.
[52]. Zhang, B., et al., *Senary refractory high-entropy alloy CrxMoNbTaVW.* Calphad, 2015. **51**: p. 193-201.
[53]. Senkov, O.N., et al., *Low-density, refractory multi-principal element alloys of the Cr–Nb–Ti–V–Zr system: Microstructure and phase analysis.* Acta Materialia, 2013. **61**(5): p. 1545-1557.
[54]. Fazakas, E., et al., *Experimental and theoretical study of Ti20Zr20Hf20Nb20X20 (X= V or Cr) refractory high-entropy alloys.* International Journal of Refractory Metals and Hard Materials, 2014. **47**: p. 131-138.
[55]. Senkov, O., et al., *Compositional variation effects on the microstructure and properties of a refractory high-entropy superalloy AlMo0. 5NbTa0. 5TiZr.* Materials & Design, 2018. **139**: p. 498-511.
[56]. Senkov, O.N., et al., *Development of a refractory high entropy superalloy.* Entropy, 2016. **18**(3): p. 102.
[57]. Xu, Z., et al., *Effects of Si additions on microstructures and mechanical properties of VNbTiTaSix refractory high-entropy alloys.* Journal of Alloys and Compounds, 2022. **900**: p. 163517.
[58]. Nie, X., M. Cai, and S. Cai, *Microstructure and mechanical properties of a novel refractory high entropy alloy HfMoScTaZr.* International Journal of Refractory Metals and Hard Materials, 2021. **98**: p. 105568.
[59]. Xiang, L., et al., *Microstructure and mechanical properties of TaNbVTiAlx refractory high-entropy alloys.* Entropy, 2020. **22**(3): p. 282.
[60]. Juan, C.-C., et al., *Enhanced mechanical properties of HfMoTaTiZr and HfMoNbTaTiZr refractory high-entropy alloys.* Intermetallics, 2015. **62**: p. 76-83.
[61]. Lee, C., et al., *Strength can be controlled by edge dislocations in refractory high-entropy alloys.* Nature communications, 2021. **12**(1): p. 5474.
[62]. Backman, L., et al., *Part I: Theoretical predictions of preferential oxidation in refractory high entropy materials.* Acta Materialia, 2020. **197**: p. 20-27.
[63]. Gorr, B., et al., *High-temperature oxidation behavior of refractory high-entropy alloys: effect of alloy composition.* Oxidation of Metals, 2017. **88**: p. 339-349.
[64]. Gorr, B., et al., *A new strategy to intrinsically protect refractory metal based alloys at ultra high temperatures.* Corrosion Science, 2020. **166**: p. 108475.

AUTHOR

Abdullah Al Masum Jabir received his master's degree on manufacturing engineering from University of Texas Rio Grande valley, Texas USA. He worked in department of defense project for 2 years as a research assistant. His research focus is high entropy alloy and additive manufacturing.

Farjana Jahan pursuing her master's degree on Applied Statistics from Western Michigan University, Michigan USA. She is working as a graduate assistant in the department. She had 10 years of experience in the industry and also in the institutional field.